Error Analysis of Boundary Conditions Using Volume Penalization in Acoustic Simulations

Yannick Schubert, Mathias Lemke
Institut für Strömungsmechanik und Technische Akustik, Technische Universität Berlin
Email: schubert@tnt.tu-berlin.de

Introduction

In previous studies, a volume penalization approach was introduced, enabling time-domain acoustic simulations for complex geometries [3]. This approach incorporates two types of penalization, allowing for the modeling of both porous and rigid materials. In this work, we conduct a more in-depth analysis of the method, focusing on numerical errors in acoustic simulations. These numerical errors are analyzed to develop effective modeling strategies and to improve the accuracy and stability of the simulations. Finally, the applicability of the method for simulating the aeroacoustics of flow around a porous-coated cylinder is investigated.

Governing equation

The fully compressible Navier–Stokes equations with volume penalization, given in Eqs. (1)–(3), serve as the governing equations for simulating not only acoustic but also aeroacoustic phenomena. The mass and momentum equations are given by:

$$\phi\partial_t(\rho) + \partial_{x_i}(\phi\rho u_i) = 0, \tag{1}$$

$$\begin{aligned}\phi\partial_t(\rho u_j) + \partial_{x_i}(\phi\rho u_i u_j) + \phi\partial_{x_j} p =& \phi\chi(u_j^{\mathrm{t}} - u_j) \\ &+ \partial_{x_i}(\phi\tau_{ij}).\end{aligned} \tag{2}$$

Assuming a constant heat capacity, the energy equation can be expressed in terms of pressure [2]:

$$\begin{aligned}\phi\partial_t\left(\frac{p}{\gamma-1}\right) + \partial_{x_i}\left(\phi\frac{\gamma u_i p}{\gamma-1}\right) =& + \phi u_i\partial_{x_i}(p) \\ &+ \partial_{x_i}(\phi\lambda\partial_{x_i}(T)) \\ &+ \phi\tau_{ij}\partial_{x_j}(u_i).\end{aligned} \tag{3}$$

In these equations, ρ, p, and u_i denote the mass density, pressure, and velocity components for $i, j = 1, 2, 3$, following the Einstein summation convention. Furthermore, λ represents the thermal conductivity, T is the temperature, and γ is the isentropic exponent. The term u_j^t corresponds to the velocity of the modeled object, which is set to zero in the following analysis.

Volume penalization

To enable the modeling of porous bodies, these equations are extended by introducing two additional parameters, the effective ϕ and the so-called Darcy term determined by χ. Similar variants of the volume penalization method are widely employed in the modeling of porous materials, enabling the representation of fluid–structure interactions within an embedded grid framework. For a detailed discussion of complex boundaries using non-conforming grids, see [4].

Effective volume (ϕ)

The effective volume fraction is defined as

$$\phi = \frac{V_{\mathrm{fluid}}}{V_{\mathrm{total}}}, \tag{4}$$

which quantifies the fraction of the volume that is accessible to the fluid, excluding the volume obstructed by the porous (or rigid) material. Accordingly, ϕ takes values in the range $0 < \phi \leq 1$. When $\phi \equiv 1$, the domain is fully occupied by fluid, and the Navier–Stokes equations retain their original form. Conversely, $\phi \to 0$ indicates a solid region, effectively modeling a rigid wall or body. Since choosing $\phi = 0$ would cause the governing equations to degenerate, only very small (nonzero) values of ϕ are used in practice. Values larger than 1 are excluded.

Darcy term ($\phi\chi(u_j^{\mathrm{t}} - u_j)$)

As part of the proposed method, a Darcy term of the form $\phi\chi(u_j^{\mathrm{t}} - u_j)$ is added to the momentum equation, where the $\chi(x_i)$ determines where and how strongly this penalization is applied. A variation of χ corresponds to a change in the permeability of the modeled material. For $\chi_s = 0$, the governing equations reduce to the Navier–Stokes equations with penalization applied only through the effective volume fraction. This term enables the modeling of length-specific flow resistivity in porous materials, as illustrated in Figure 2. To demonstrate, a porous probe is simulated using only the Darcy term ($\phi = 1$), as shown in Figure 1. By applying a constant flow in the x-direction, the flow resistivity $r = \frac{\Delta p}{u_\infty L}$ can be determined from the pressure drop across the material Δp, the inflow velocity u_∞ and the material length L. Varying the value of χ allows for the representation of different porous materials, see Figure 1. The limit $\chi \to \infty$ corresponds to a rigid wall [1]. However, increasing χ excessively may lead to a reduction of the allowable time step to maintain numerical stability. By appropriately selecting the spatially varying parameters χ and ϕ, porous and solid objects with different material properties can be represented.

Smoothing

To ensure numerical stability using this volume penalization approach, transitions between fluid and modeled bodies are carefully smoothed over a few grid points. One way to achieve this smoothing is by employing a hyperbolic tangent function. For the effective volume, this

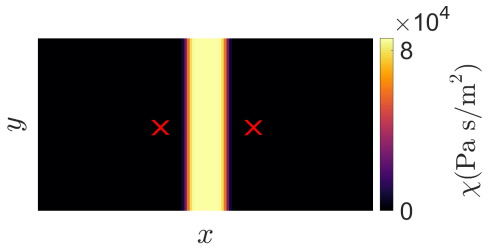

Figure 1: Visualization of an exemplary penalization setup used to measure the flow resistivity of a porous probe. Red crosses indicate microphone positions.

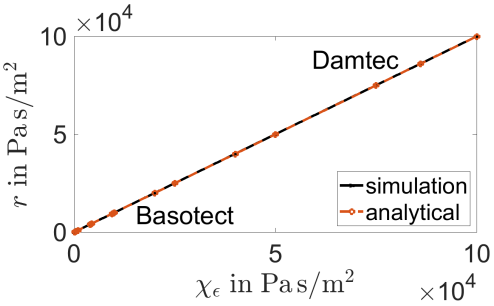

Figure 2: Comparison between analytical (black) and numerical (orange) results for flow resistivity.

results in:

$$\phi(x_i) = 1 - (1 - \phi_\epsilon)\frac{\tanh((x_i - x_0)/\delta_\phi) + 1}{2}, \quad (5)$$

where δ_ϕ represents the smoothing width, and ϕ_ϵ is the residual volume fraction within the wall. Similarly, the smoothing of the permeability is given by:

$$\chi(x_i) = \chi_\epsilon \frac{\tanh((x_i - x_0)/\delta_\chi) + 1}{2}, \quad (6)$$

where δ_χ determines the smoothing width for permeability, and χ_ϵ is the residual permeability at the wall.

Framework and Numerical Setup

The governing equations are implemented and solved using the in-house computational framework CRUNA (Compressible Reactive Unsteady Navier–Stokes Adjoint). The code is parallelized for high-performance computing (HPC) and optimized for computational efficiency. CRUNA is publicly available at: `https://github.com/cruna-toolkit`.

To investigate the influence of the modeling parameters and their inter-dependencies, a simplified one-dimensional test case involving acoustic wave reflection at a rigid wall is considered. The setup is illustrated in Figure 3. Several configurations are examined for representing the wall: (i) penalization using only the Darcy term, (ii) penalization through the effective volume fraction alone, and (iii) various combinations of both approaches. The computational domain spans from $x = 0$ to $x = 3\,\mathrm{m}$ and is discretized using equidistant grid points along the x-axis. The error is evaluated using a primary resolution of $N_1 = 769$ points. To estimate its convergence rate, a second simulation with a finer resolution of $N_2 = 1025$ points is used.

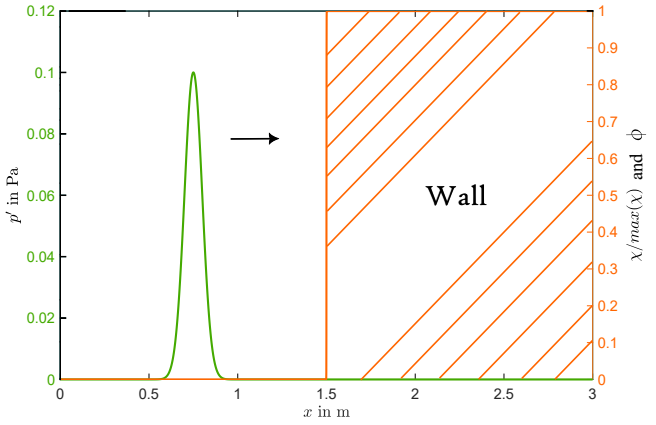

Figure 3: Illustration of a one-dimensional simulation of acoustic wave (green) reflection at a rigid wall (orange) modeled using volume penalization.

For the numerical solution of the extended, compressible Navier-Stokes equations, a compact, implicit fourth-order scheme is employed for spatial derivatives. Temporal integration is performed using the classical fourth-order Runge-Kutta method. The time step is set to $\Delta t = 7.9719 \times 10^{-6}\,\mathrm{s}$, corresponding to a Courant–Friedrichs–Lewy (CFL) number of 0.7.

In addition to the volume penalization, non-reflecting boundary conditions are applied using characteristic boundary treatment. The initial condition consists of an adiabatic pressure pulse positioned in front of the wall.

To quantify the error, the following expression is used:

$$\text{error} = \int \frac{|p'_{\text{ref}} - p'_{\text{penalized}}|}{|p'_{\text{ref}}|}\,\mathrm{d}x \quad (7)$$

Here, p'_{ref} represents the discretely exact solution obtained from a mirror-source reflection, while $p'_{\text{penalized}}$ denotes the solution computed using volume penalization, evaluated at $x = 1.5\,\mathrm{m}$.

Results Error Analysis

In Figure 4 the error with respect to variations of the amplitudes of ϕ_ϵ and χ_ϵ is shown. The smoothing parameter for both penalization functions is set to $1.25\Delta x$. As expected, the maximum error occurs at $\phi_\epsilon = 1$ and $\chi_\epsilon = 0$, which corresponds to the absence of any wall. Physically consistent behavior is observed: when the porosity remains constant at $\phi_\epsilon = 1$, the error decreases with increasing permeability χ_ϵ. Conversely, when no permeability is modeled ($\chi_\epsilon = 0$) but the porosity ϕ_ϵ is reduced, the error also decreases. The smallest error is achieved when ϕ_ϵ is minimized and $\chi_\epsilon = 0$. In this case, the method attains the highest observed convergence rate of $\mathcal{O}(\Delta x^3)$. In contrast, using permeability alone (χ only) results in a significantly lower convergence rate of $\mathcal{O}(\Delta x^{0.5})$. For each value of the effective volume, one can observe convergence toward a specific error value as the spatial resolution increases. This convergence occurs more rapidly for larger values of ϕ_ϵ, which explains

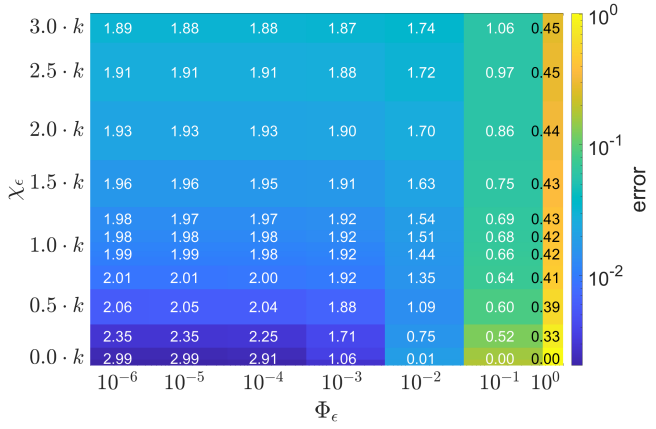

Figure 4: Visualization of the error (7) as a function of the porosity amplitude ϕ and permeability amplitude χ, with smoothing parameters δ_ϕ and $\delta_\chi = 1.25\Delta x$. The white and black numbers within the cells indicate the order of convergence of the error. The scaling factor k is defined as $k = \frac{s}{\Delta t}\mathrm{Pa\,s\,m^{-2}}$.

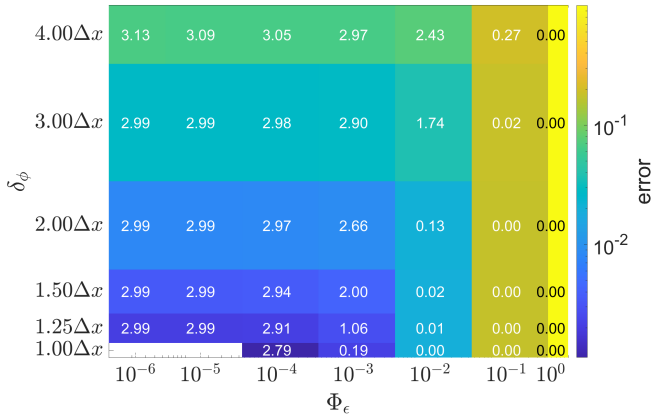

Figure 5: Error distribution as a function of ϕ_ϵ and δ_ϕ. White regions indicate parameter combinations that resulted in unstable simulations. The white and black numbers within the cells represent the order of convergence of the error.

the lower apparent convergence order for the computed resolution. However, before reaching the converged error value, the order of convergence remains comparable to that observed for very small values of ϕ_ϵ.

In Figure 5, the error is displayed in relation to the amplitude ϕ_ϵ and the smoothing parameter δ_ϕ. For large values of ϕ_ϵ, the effect of δ_ϕ on the error is minimal. In contrast, for small ϕ_ϵ, the error decreases as δ_ϕ is reduced. However, the overall order of convergence remains nearly unchanged. Notably, when δ_ϕ becomes too small for very low values of ϕ_ϵ, numerical instabilities arise, as indicated by the missing regions in the figure. Thus, the optimal selection of the modeling parameters for representing a rigid wall should be as close as possible to the actual configuration while maintaining numerical stability.

Figure 6 illustrates the error as a function of the amplitude χ_ϵ and the smoothing parameter δ_χ. As expected, the largest errors occur for small permeability values χ. The error decreases as χ_ϵ increases, though this effect diminishes for larger values of δ_χ. The maximum achieved convergence order is 0.5 at the point of minimum error.

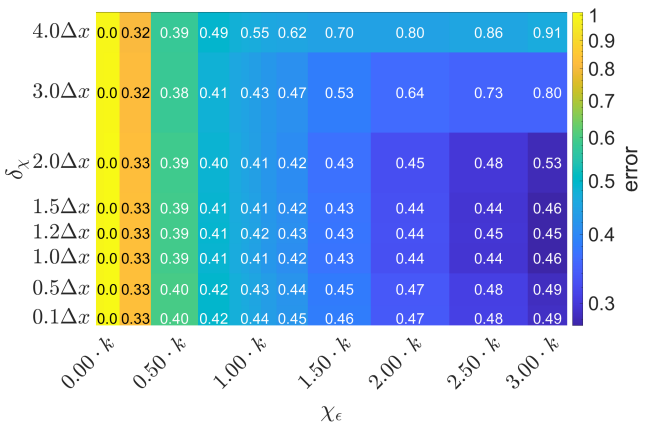

Figure 6: Visualization of the error as a function of χ_ϵ and δ_χ. The white and black numbers within the cells correspond to the order of convergence of the error. The factor k is defined as $k = \frac{s}{\Delta t}\mathrm{Pa\,s\,m^{-2}}$.

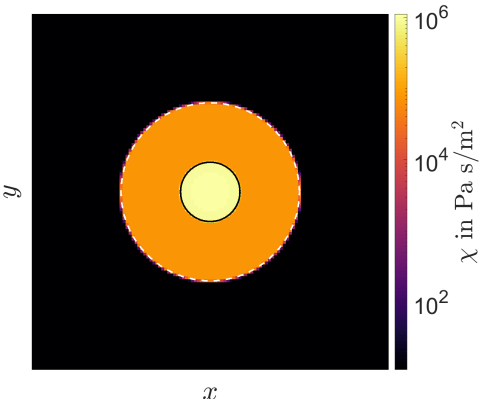

Figure 7: Graphical representation of the Darcy term penalization applied to a porous-coated cylinder.

In summary, both penalization approaches and their combination are effective for representing rigid objects in acoustic simulations. By selecting the modeling parameters as closely as possible to the physical configuration, the best results can be achieved.

Application to Porous Coated Cylinder

The proposed volume penalization approach is effective not only for simulating the acoustics of rigid objects but also for modeling porous materials, capturing flow dynamics, and accurately representing the associated aeroacoustic phenomena. In particular, it can be applied to investigate sound generation in a flow around porous-coated cylinders. This application necessitates the use of both penalization parameters to accurately represent the flow resistivity and porosity of the coating material, as illustrated in Figures 7 and 8.

As a first step in evaluating the influence of individual modeling parameters and verifying the validity of the approach, a sensitivity study is performed. The sensitivity S of a quantity q, such as the Strouhal number Sr, with

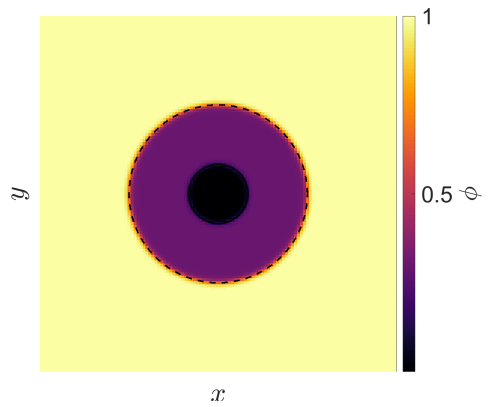

Figure 8: Graphical representation of the effective volume penalization applied to a porous-coated cylinder.

Parameter	$\overline{S}_{L_p}$ in %
χ_{porous}	21.71
ϕ_{porous}	−27.87
δ_χ	−0.68
δ_ϕ	−2.96

Table 1: Sensitivity of modeling parameters.

respect to a parameter α and its variation $\Delta\alpha$, is defined as:

$$S = \frac{q(\alpha + \Delta\alpha) - q(\alpha)}{\Delta\alpha} \cdot \frac{\alpha}{q(\alpha)}. \tag{8}$$

In this context, sensitivities are evaluated with respect to the sound pressure level amplitude S_{L_p} at the peak frequency. Simulations are performed with small perturbations of the modeling parameters. The reported sensitivity values represent averages over the simulation results. Similar to the rigid wall case, it is observed that for the aeroacoustic simulation of the porous-coated cylinder, the parameters describing the physical properties of the material play a crucial role. This further underscores the validity of the approach. A more detailed discussion of the simulations and additional results is presented in [5], which has been submitted to Computer & Fluids and is currently under review.

Conclusion and Outlook

The proposed volume penalization approach has been successfully applied and investigated for both acoustic and aeroacoustic phenomena. It relies primarily on two parameters: the effective volume fraction (porosity) ϕ and the Darcy term (permeability) χ.

The conducted parameter study enables the evaluation of the impact of varying the amplitude and smoothing properties of these parameters, with the results compared to a rigid wall test case. The analysis reveals that porosity (ϕ) is much more effective in representing acoustically rigid walls, as it results in lower errors and achieves a higher order of convergence. Furthermore, ϕ places fewer restrictions on time integration stability when compared to permeability (χ).

Porous bodies with varying acoustic characteristics can be effectively modeled and simulated using the proposed approach, which is grounded in physical principles. The reliability of this method was further validated through its successful application to simulate sound generation from flow around a porous-coated cylinder.

The underlying framework, CRUNA, is available on GitHub. Due to its high accuracy, both fluid dynamic and acoustic effects can be captured precisely within a single simulation. Its strong scalability in parallel execution ensures excellent performance.

The spatial variability of the quantities ϕ and χ provides the approach with a high degree of flexibility for modeling. This enables precise adaptation and representation of material properties at each grid point, making the method especially suitable for geometry optimization.

Future work will focus on solving this high-dimensional optimization problem using an adjoint-based method.

References

[1] Mathias Lemke, Vincenzo Citro, and Flavio Giannetti. External acoustic control of the laminar vortex shedding past a bluff body. *Fluid Dynamics Research*, 53(1):015506, feb 2021.

[2] Mathias Lemke, Arne Hölter, and Stefan Weinzierl. Physics-informed identification and interpolation of the directivity of sound sources. *IEEE Transactions on Audio, Speech and Language Processing*, 33:372–385, 2025.

[3] Mathias Lemke and Julius Reiss. Approximate acoustic boundary conditions in the time-domain using volume penalization. *The Journal of the Acoustical Society of America*, 153(2):1219, February 2023.

[4] Julius Reiss. Pressure-tight and non-stiff volume penalization for compressible flows. *Journal of Scientific Computing*, 90(3), January 2022.

[5] Yannick Schubert, Ennes Sarradj, and Mathias Lemke. A volume penalization method for acoustic and aeroacoustic simulation of solid and porous bluff bodies. 2025.